Characterization of Structural Transition and Heterogeneity under Compression for Liquid Al₂O₃ Using Molecular Dynamics Simulation

Pham Huu Kien [1] , Tran Thi Quynh Nhu [1, 2], Giap Thi Thuy Trang [1*]

[1] Department of Physics, Thainguyen University of Education, No. 20 Luong Ngoc Quyen, Thainguyen, Viet Nam.

[2] Tuyen Quang High School for Gifted Students, Tran Hung Dao Street, Tuyenquang, Viet Nam

Abstract

We have performed a simulation of the structural transition and Structural Heterogeneity (SH) in liquid Al₂O₃ at 3500 K, in the range of 0–100 GPa. The results confirmed that the network structure of liquid alumina is built mainly from AlO_x (x = 3, 4, 5, 6, 7) units, which are related to each other through the common oxygen atoms. The existence of separate AlO_3-, AlO_4-, AlO_5-, AlO_6- and AlO_7- phases, where SH of the network structure can be sufficiently determined, besides, the existence of separate phases is clarified for SH in the liquid of Al₂O₃. In particular, at a pressure below 10 and beyond 20 GPa, AlO_x units are uniformly distributed in the space and non-uniformly distributed in the range 10-20 GPa. Our study is expected to contribute to a simple way to determine the structural heterogeneity and diffusion coefficients of oxide systems.

Keywords: Molecular Dynamics; Liquid; Network Structure; Phase; Cluster; Structural Transition.

1. Introduction

Recently, Al₂O₃ has become well-known as the refractory ceramic oxide used in numerous applications, such as electronic devices, optics, and mechanical engineering, biomedical engineering, and cutting tools. Thus, liquid Al₂O₃ has become of great interest to researchers through both experimental and theoretical developments [1-9]. For instance, by using X-ray diffraction and scattering, Waseda et al. [10] and Ansell et al. [11] revealed that the two first peaks of the total radial distribution function (RDF) located at 2.0 and 2.8 Å as the density of 3.01 g.cm⁻³ and 1.76, 3.08 Å as the density of 3.175 g.cm⁻³. The averaged coordination number of the Al-O pair is equal to 4.5 ± 0.1. Besides, Hennet et al. [12] found out the first-, second- and third-peaks of RDF $g_{Al-O}(r)$ are located at 1.80 ± 0.02, 3.18 ± 0.06 and 4.36 ± 0.01 Å, respectively. These averaged coordination number of Al-O pair is approximately estimated to be 4.3 ± 0.05. To support experimental methods, simulation is also a powerful method to investigate the microstructure of melts, especially at high-temperature and/or pressure conditions [13-19]. According to the first-principles molecular dynamic (MD) simulations, Verma et al. [8] determined that the liquid Al₂O₃ is more sensitive to the applied compression than the temperature. The coordination number of Al atoms includes various species with disappearing three- and four-coordinated and appearing six- and seven-coordinated since the liquid is compressed. Skinner et al. [20] indicated that the melt consisted predominantly of AlO_4 and AlO_5 units. It can be noted that Al-O-Al connections of 83% are involved in the corner-sharing polyhedra, compared to 16% for the edge-sharing polyhedral. Miguel et al. [21] found that more than 50% of Al atoms are tetrahedral coordinated at four different temperatures. According to Hoang et al.

[22] and Hung et al. [23], they showed the clear evidence of structural transition in liquid Al_2O_3 from a tetrahedral to an octahedral network. The voids created a very large hole with a volume five times bigger than that of the aluminum atom. Other simulations [24, 25] showed that the phase regions of liquid Al_2O_3 strongly depend on compression. The mobility of atoms in different phases is different; the AlO_6-phase forms immobile regions. At low temperatures, the coexistence of AlO_4-, AlO_5-, and AlO_6-phases is the origin of the spatially dynamical heterogeneity.

However, up to now, the development of structural transition and SH under compression for liquid Al_2O_3 is still intensively improved. In the present work, a large-scale MD simulation of an Al_2O_3 system consisting of 5500 atoms was performed. The structural characteristics such as the RDF, characteristics of AlO_x and OAl_y units, visualization of simulation data have been clarified for the structural transition and SH in liquid Al_2O_3 under compression condition.

2. Calculation Method

Models of liquid Al_2O_3 consisting 5500 atoms (2200 Al- and 3300 O-atoms) are constructed by MD simulation at 3500 K, in the range 0-150 GPa, with boundary conditions for all three dimensions. The Born-Mayer potential, which has been successfully used for structural and dynamic simulation of Al_2O_3 systems, was employed in this work. The detail about the Born-Mayer potential can be referred from Kovarik et al. (2021), Hoang & Oh (2004), and Belashchenko (1997) study [4, 15, 26]. The MD program is coded in the C language and uses the Verlet algorithm to integrate the motion equations. In this case, MD time step is selected to be 0.47 fs. Initial configuration of the model is created by randomly sowed all atoms in the simulation space. The model is heated up to 6000 K and zero pressure. Then, the model is cooled down to 3500 K within 2×10^4 time steps with the cooling rate of 2.0 K/ps. After that, a long relaxation (5×10^6 time steps) has been done in isothermal-isobaric (*NPT*) ensemble to equilibrate the model at 3500 K and zero pressure. From this well-equilibrated liquid Al_2O_3 at 3500 K and zero pressure, the proposed models at different pressures (5-100 GPa) which are labeled as M_1, M_2…M_{11}, respectively (as seen in Table 1). These models were constructed by relaxing again within 5×10^6 time steps to reach the equilibrium in isothermal-isobaric *NPT* ensemble. The structural characteristics of each model are determined by averaging 1000 configurations during the last 5×10^4 MD steps. To calculate the clusters as well as coordination number, the cutoff distance is chosen based on the minimum position after the first peak of the RDF. Remarkably, for the Al-O pair, the cutoff distance is 2.54 Å.

3. Result and Discussion

3.1. The Structural Transition under Compression

The characteristics of the constructed models, experimental, calculation and other simulation are listed in Table 1. Obviously, the major changes are a shift of distance r_{ij} to bigger value for Al-O pair and smaller value for Al-Al, O-O pairs with increasing of the applied pressure. The coordination number strongly increases with increasing of pressure. Namely, at 0 GPa, the averaged coordination numbers for Al-Al, Al-O, O-Al and O-O pairs were found to be 7.71, 4.25, 2.83 and 10.64, respectively. These numbers increased to be 13.68, 6.54, 4.36 and 16.77 as pressure increases from 0 to 100 GPa. Also, the BKS model reproduces well the structural data obtained from experimental and simulated data from Refs. [1, 2, 7, 8, 20, 22]. Thus, the prepared models are reliable to investigate the structural transition and SH of liquid Al_2O_3.

Table 1. The structural characteristics of constructed models at different pressures, experimental and simulation data. Here T, P, ρ are temperature, pressure and density, respectively; r_{Al-Al} , r_{Al-O}, r_{O-O} is the inter-atomic distance for Al-Al, Al-O and O-O pair, respectively; z_{Al-Al}, z_{Al-O} z_{O-Al}, z_{O-O} are the average coordination number for Al-Al, Al-O, O-Al and O-O pair, respectively.

| Models	T (K)	P (GPa)	ρ (g/cm^3)	r_{Al-Al} (Å)	r_{Al-O} (Å)	r_{O-O} (Å)	z_{Al-Al}	z_{Al-O}	z_{O-Al}	z_{O-O}
M_1	3500	0.01	2.78	3.14	1.68	2.78	7.71	4.25	2.83	10.64
M_2	3500	5	-	3.16	1.72	2.70	11.75	5.30	3.54	13.94
M_3	3500	10	-	3.14	1.74	2.70	11.81	5.37	3.58	14.04
M_4	3500	15	-	3.10	1.70	2.70	11.89	5.43	3.62	14.15
M_5	3500	20	-	3.12	1.72	2.64	11.97	5.51	3.67	14.36
M_6	3500	25	-	3.08	1.72	2.62	12.02	5.55	3.70	14.43
M_7	3500	30	-	3.08	1.72	2.60	12.20	5.63	3.76	14.66
M_8	3500	40	-	3.08	1.72	2.56	12.31	5.80	3.87	15.19
M_9	3500	60	-	3.00	1.70	2.52	12.42	5.85	3.90	15.37
M_{10}	3500	80	-	2.84	1.72	2.50	13.74	6.45	4.30	16.26
M_{11}	3500	100	-	2.88	1.72	2.46	13.68	6.54	4.36	16.77
Exp. [11]	2500	-	2.81	3.25	1.78±0.05	2.84	-	4.20±0.3	-	-
Exp. [1]	2200-2650	-	3.17	-	1.732	3.08	-	4.40±1.0	-	-
Exp. [20]	2400±50	-	-	3.15	1.80	2.82	8.85	4.40	2.93	12.90
Sim. [22]	2500	0.05	2.80	3.20	1.77	2.80	8.00	4.20	2.80	7.44
Cal. [8]	4000	-	3.683	3.02	1.79	2.61	12.4	5.52	3.69	15.60
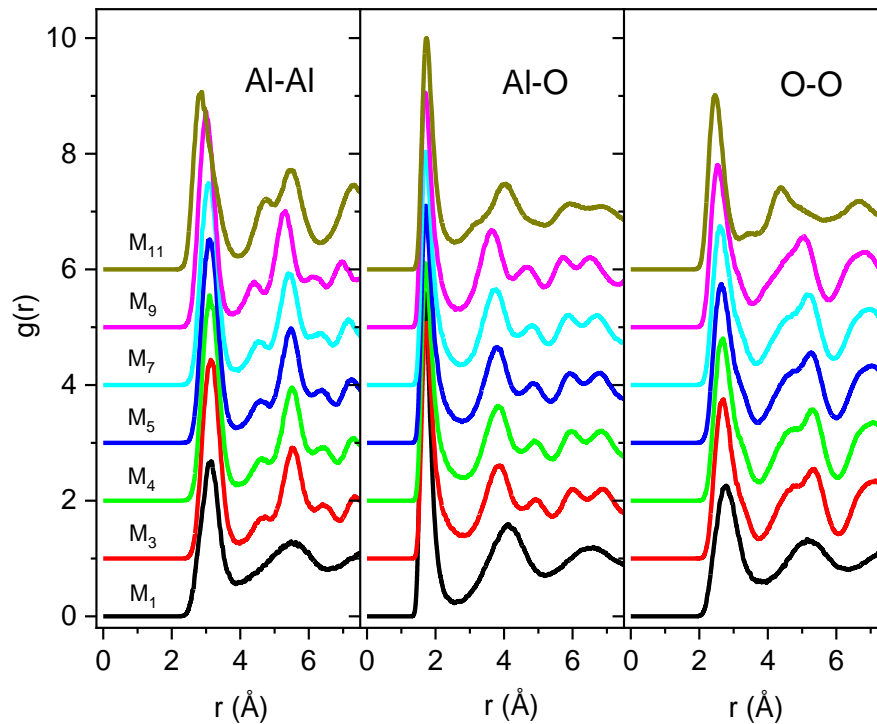
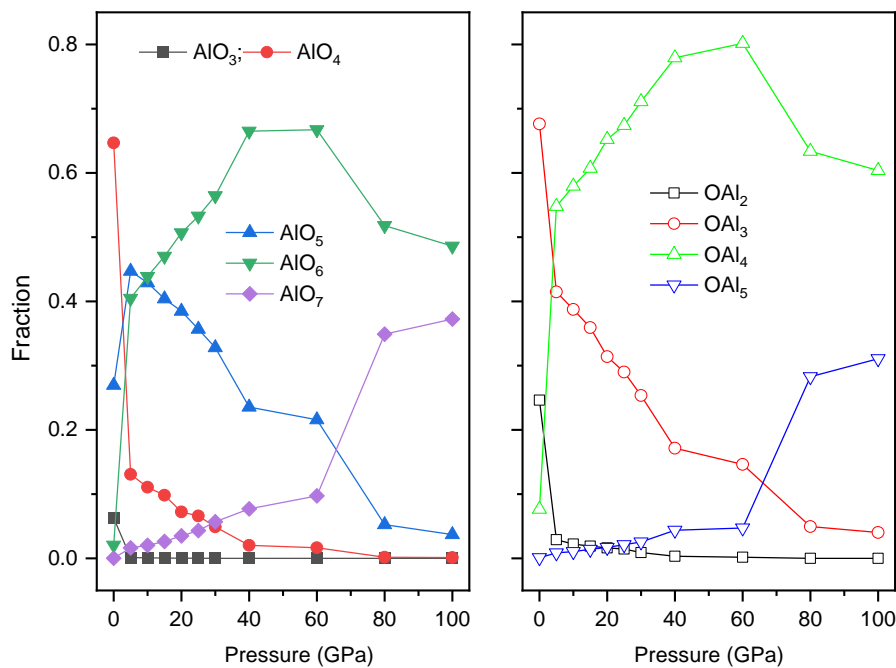**Figure 1. The radial distribution function of liquid Al₂O₃ at different pressures**

Figure 2. Dependence of coordination number distribution on applied pressure for: AlOₓ (left) and OAlᵧ (right)

Figure 1 displays the RDFs $g_{Al-O}(r)$, $g_{Al-Al}(r)$ and $g_{O-O}(r)$ at different pressures. It can be seen that, under compression for the $g_{Al-O}(r)$, the position of the first peak is displaced to the right-hand side and their magnitudes are significantly decreased. In contrast, for the $g_{O-O}(r)$, and $g_{Al-Al}(r)$, the position of the first peak is displaced to the left-hand side and their magnitudes are independent on the increased pressure. Based on above analyses, the network structure of liquid Al₂O₃ is changed insignificantly both of intermediate- and short-range order structure, which is depended on the compression.

Next, we clarified the origin of the change of the network structure of liquid Al₂O₃ under compression via the characteristics of AlOₓ and AlOᵧ basic units. As shown in Figure 2, the fraction of AlO₃, AlO₄, OAl₂, and OAl₃ are decreased with increasing pressure while the fraction of AlO₇ and OAl₅ are increased. Specially, the fraction of AlO₅,

AlO$_5$ and OAl$_4$ creates a maximum value at 5 GPa for AlO$_5$ and at 50 GPa for AlO$_5$ and OAl$_4$. This phenomenon indicated a transformation in local environment of Al ions from tetrahedral- to octahedral- coordination at 5 GPa and beyond 50 GPa, which leads to the system becomes to be denser. This result can be regarded as the bond length between O and O in AlO$_5$ units is larger than the one in AlO$_6$ and smaller than the one in AlO$_4$.

The bond angle and length distribution calculated separately for each type of AlO$_x$ basic units are shown in Figure 3 and 4. It showed that the angle-distributions are almost independent on pressure for AlO$_5$. However, the deviations in the magnitude and position of main peak are observed in cases of AlO$_4$ and AlO$_6$ (as depicted on the left side of Figure 3). Furthermore, on the right side of Figure 3, the bond-length distribution for AlO$_4$ and AlO$_6$ are significantly depended on the pressure, which causes the magnitude- and position-deviations. Clearly, under compression, the shape and size of AlO$_4$, AlO$_5$ and AlO$_6$ units are changed and little distorted. As presented in Figure 4, the angle distributions of OAl$_2$, OAl$_3$ and OAl$_4$ units are not identical (depended on pressure). It means that the topology structure of basic-structural units is also dependent on pressure. It can be concluded that the network structure of liquid Al$_2$O$_3$ is formed by order parameters as follows: i/ the order parameters related to the short-range order (SRO), including AlO$_3$, AlO$_4$, AlO$_5$, AlO$_6$ and AlO$_7$ units; ii/ the linkage OAl$_2$, OAl$_3$ and OAl$_4$ are order parameters, which are related to the intermediate-range order (IRO). At low-pressure state, the number of linkages OAl$_3$ and OAl$_4$ is small. At high-pressure state, as most of linkages are OAl$_3$ and OAl$_4$, the IRO is characterized by network of interconnected tetrahedra by the edge-sharing. Clearly, the OAl$_2$ linkages connected among AlO$_3$ and AlO$_4$ units causes a cluster of AlO$_3$ and AlO$_4$ units. In other words, this cluster is formed by the interconnected tetrahedra and the corner-sharing, which characterizes the low-density phase. The network structure of high-density phase is produced from OAl$_3$ and OAl$_4$ linkages. Consequently, the OAl$_3$ and OAl$_4$ linkages connect among AlO$_x$ (x = 5, 6, 7) units forming a cluster of AlO$_5$, AlO$_6$ and AlO$_7$ units.
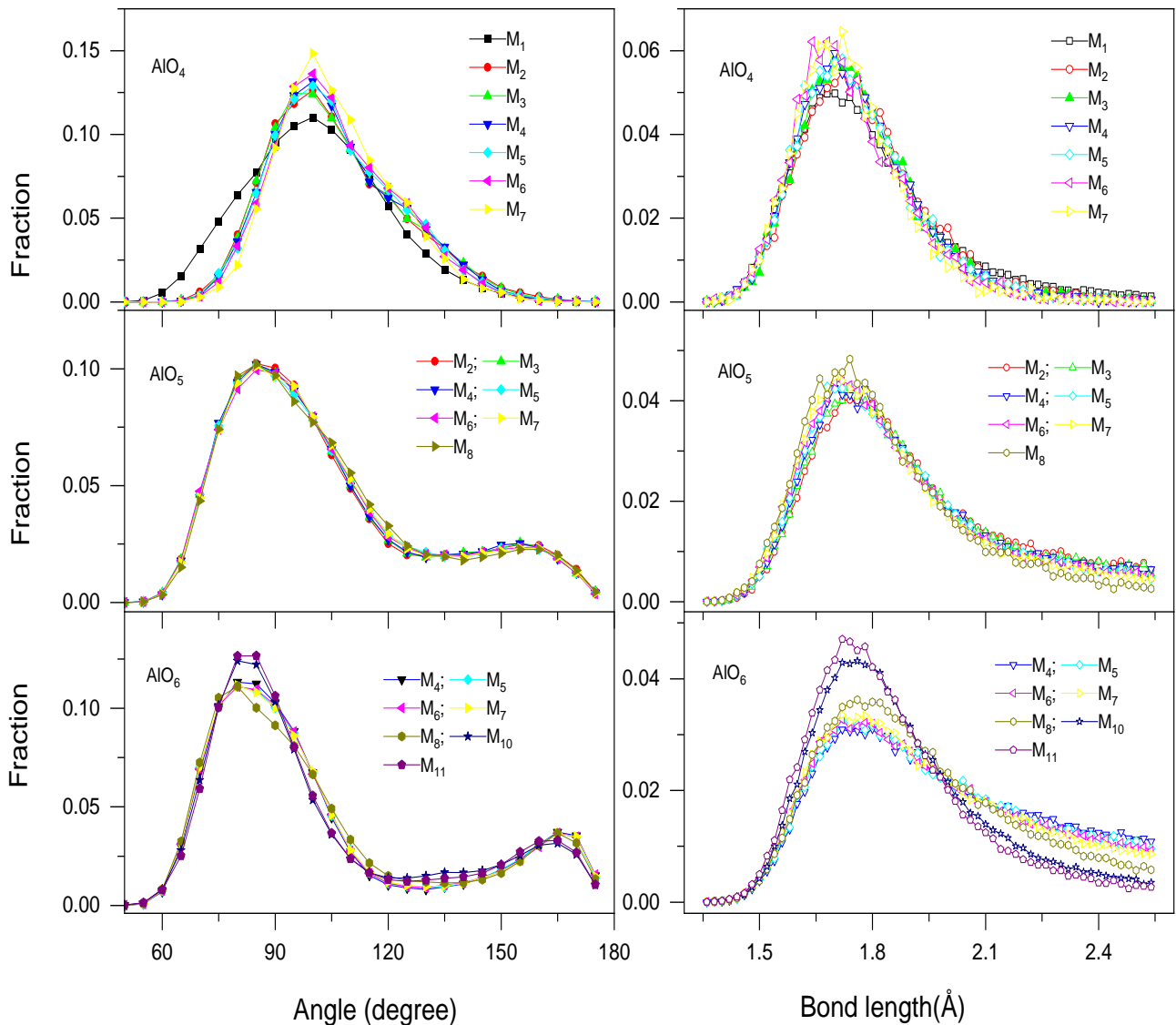

Figure 3. Bond angle O-Al-O (left) and length (right) distribution in coordination units AlO$_x$ at different pressures
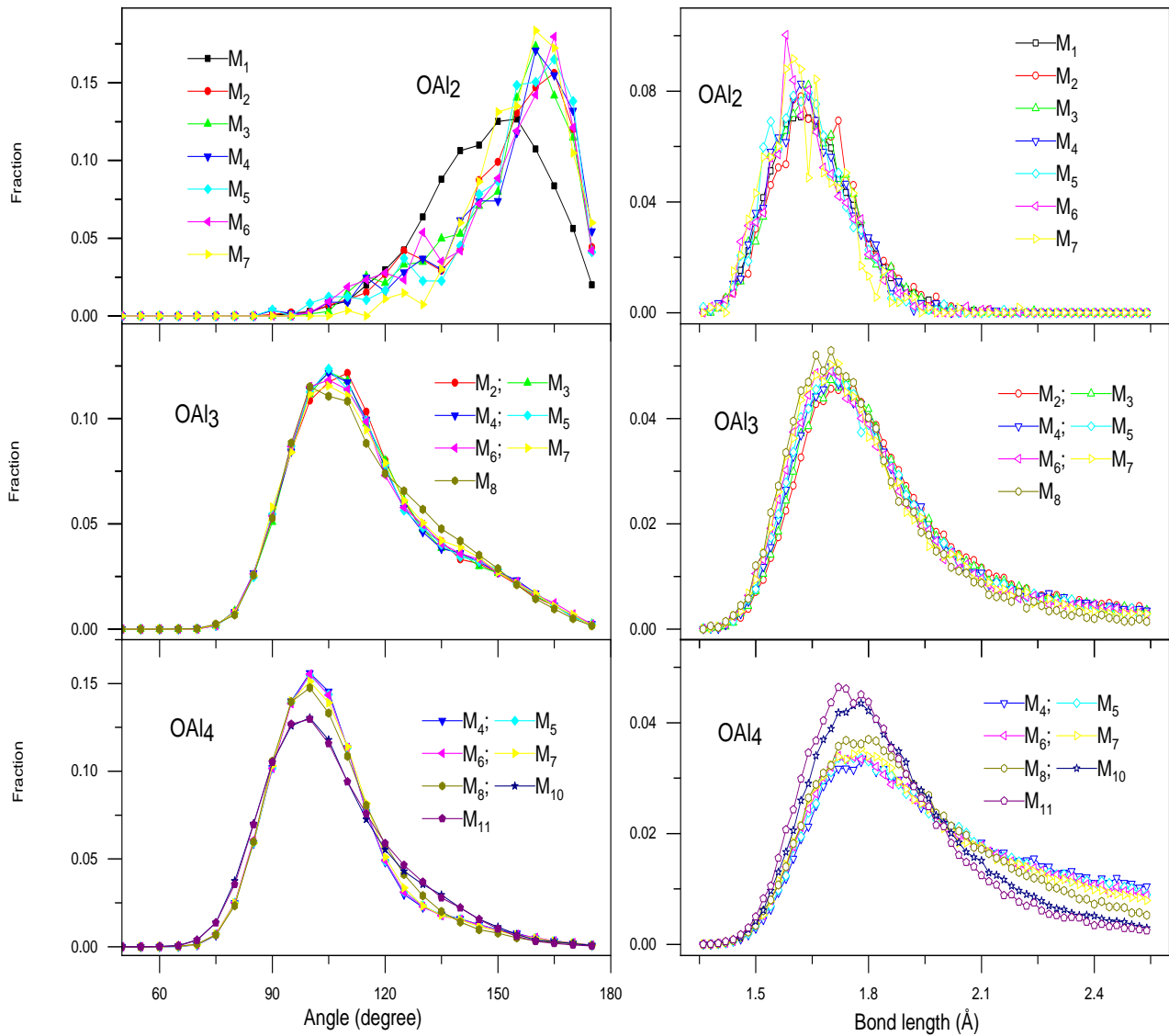
Figure 4. Bond angle Al-O-Al (left) and length (right) distribution in coordination units OAl$_y$ at different pressures

3.2. The structural heterogeneity under compression

The SH for liquid Al$_2$O$_3$ through the analysis Voronoi volume of atoms, the link-cluster function, visualization of simulation data and the consideration the mean square displacement (MSD) of atoms are clarified in this part. As presented in Figure 5, in comparison with Al, the fraction curve of O ion spreads in wider intervals. When the pressure increase, the graphs shift to the left. This phenomenon indicated that O occupies significantly larger volume compared to Al result, therefore, the Voronoi volume is decreased with increasing pressure. Clearly, Figure 6 displays the average Voronoi volumes of Al- and O-atoms under compression. Consequently, $<v_{Al}>$ and $<v_O>$ are monotonously decreased, in which $<v_O>$ is decreased stronger than $<v_{Al}>$. These results confirmed that the IRO is modified stronger than the SRO upon compression.

To characterize the cluster of atoms, we proposed the link-cluster function $F_{link}(r,t)$ and the exploited calculated algorithm can be found from Hung et al. (2018) and Lan et al. (2019) study [27, 28]. Here, we considered sets of mobiles, immobiles and random atoms (SMA, SIMA and SRA), which contains total atoms of 20%. It can be noted that the SMA has the mean-square-displacement (MSD), which is larger than that of remaining atoms. Conversely, the SIMA has the MSD smaller than that of remaining atoms. The SRAs are randomly chosen from the proposed models. The atoms of SMA, SIMA and SRA are determined from the atom position in the configuration at $t = 2 \times 10^5$ time steps. Figure 7 shows the link-cluster function $F_{link}(r,t)$ at 5, 15, 20 and 80 GPa. It is clearly seen that, at 5 and 80 GPa, the function $F_{link}(r,t)$ for SMA, SIMA and SRA is very identical. As r varies from 1.5 to 2.55 Å, $F_{link}(r, t)$ for SMA, SIMA and SRA drops drastically to 689, 745; 521 at 15 GPa and 663, 740 and 551 at 20 GPa, respectively. Meanwhile, SIMA, SMA and SRA drops drastically to the same values, namely, to 558, 615 and 648 at 5 GPa and 521 at 15 GPa; 331, 353 and 325 at 80 GPa, respectively. Moreover, with further increasing r, a shoulder is appeared, then $F_{link}(r, t)$ is decreased gradually. We concluded that at 5 and beyond 80 GPa, AlO$_x$ units are uniformly distributed in

the space. Meanwhile, in the range 15-20 GPa, the spatial distribution of AlO_x units is non- uniformly. This is caused by strongly rearrangement of atoms in the range 10-20 GPa compared to that of below 15 and beyond 20 GPa.
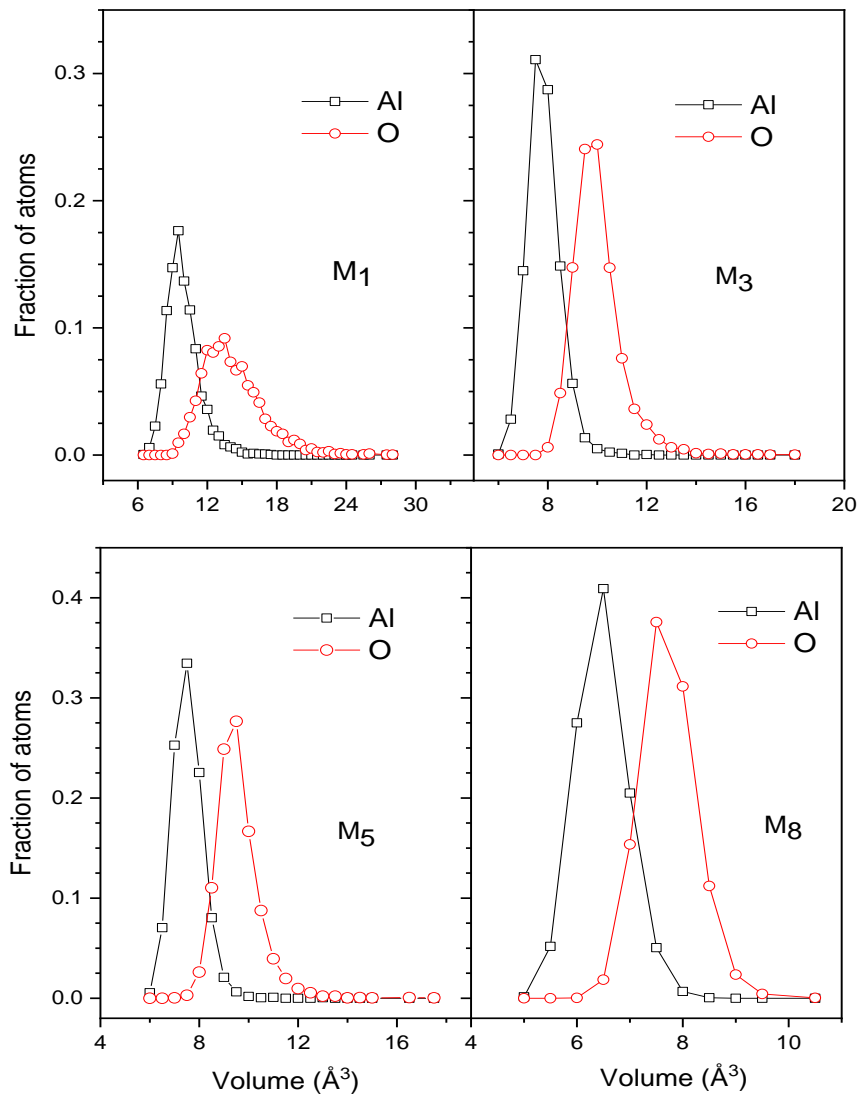

Figure 5. Dependence of fraction of Al and O on Voronoi volume at 0, 10, 20 and 40 GPa. Fraction of Al, O is given respectively by $m(v_{Al})/m_{Al}$ and $m(v_O)/m_O$ with $m(v_{Al})$, $m(v_O)$ is the number of Al and O having volume v_{Al} and v_O, respectively. m_{Al} and m_O are the total number of Al and O, respectively.
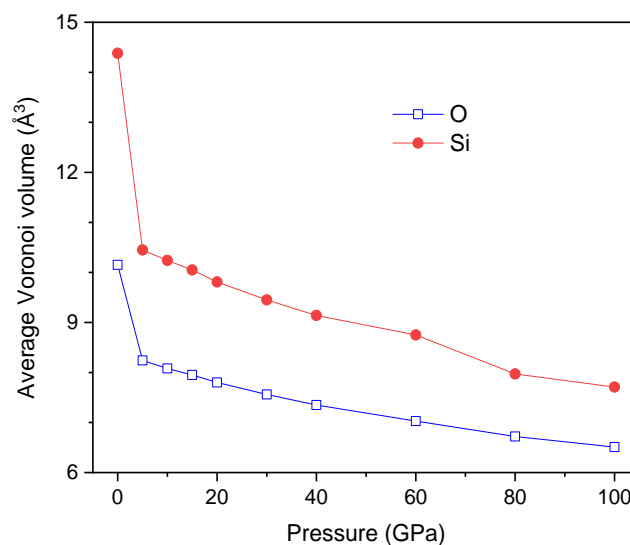

Figure 6. Pressure dependence of average Voronoi volume of Al-, O-atom
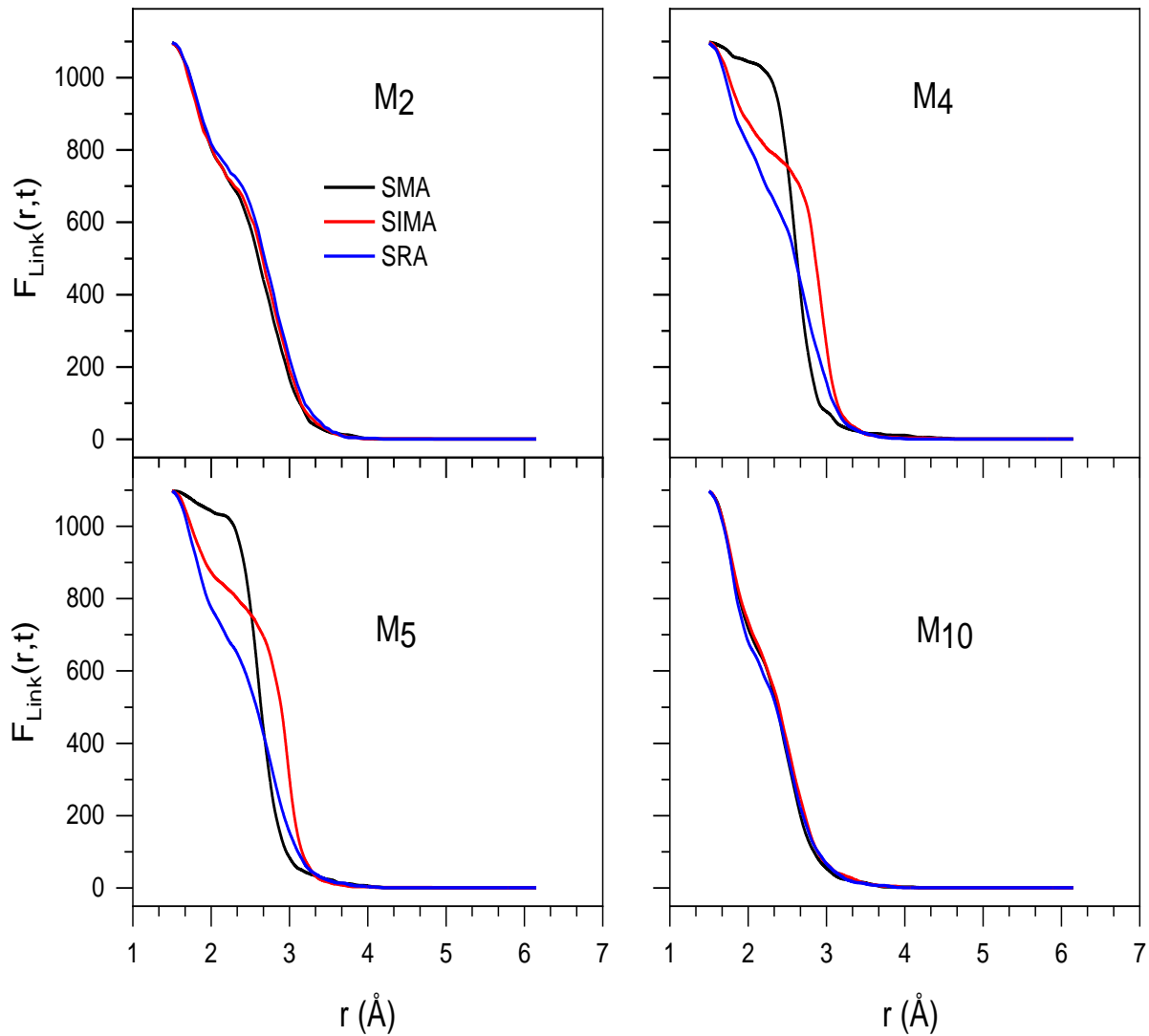
Figure 7. The link-cluster function at 5, 15, 20 and 80 GPa

Figure 8 displays the partial distribution of AlO_x in the liquid Al_2O_3 at different pressures. Obviously, the distribution of AlO_x units is not uniform and it tends to form clusters (subnets) of AlO_3, AlO_4, AlO_5, AlO_6 and AlO_7. It means that the structure of liquid Al_2O_3 comprises the mixture of AlO_3, AlO_4, AlO_5, AlO_6 or AlO_7 clusters. Namely, the structure of liquid Al_2O_3 is the mixture of regions with different SRO. The structure of liquid Al_2O_3 consists of structural phases is that AlO_3-, AlO_4, AlO_5-, AlO_6- or AlO_7 -phases, AlO_x (x = 3, 4, 5, 6, 7) phases are formed by the AlO_x units, respectively. It can be seen that at 0 GPa, the regions with AlO_3, AlO_4, AlO_5 -phase are linked to each other to create a large region with the expanse almost whole model. The region with AlO_6- and AlO_7-phases is small and localized at different locations leading to separated regions. As pressure is increased, the regions with AlO_5-, AlO_6- and AlO_7 -phases are expanded and the regions with AlO_3 and AlO_4-phase are shrunk. At pressure of 10, 20 GPa, the regions with AlO_5- and AlO_6-phase are expanded the whole model. At pressure of 100 GPa, the regions with AlO_3-, AlO_4-, AlO_5-phases are shrunk, whereas the regions with AlO_6- and AlO_7 -phases are expanded almost the whole model. It is noted that the coexistence of different phases in network-forming liquids under compression can be examined by the neutron and X-ray diffraction experiments [29, 30].

To clarify the distribution of AlO_x (x = 3, 4, 5, 6, 7) units in proposed models, the structures at different pressures are visualized in the 3D space (as shown in Figure 9). At 0 GPa, most of structural units are AlO_4, AlO_5 and some AlO_3, AlO_6 and AlO_7 units. The spatial distribution of AlO_4, AlO_5 is not uniform but it tends to form AlO_4- and AlO_5-clusters. At pressure of 10, 15, 20 and 60 GPa, most of structural units are AlO_5, AlO_6 and they also tend to form AlO_5- and AlO_6-clusters. At pressure of 100 GPa, in particular, most of structural units are AlO_6, AlO_7 and they are also tended to form of AlO_6-, AlO_7-clusters.
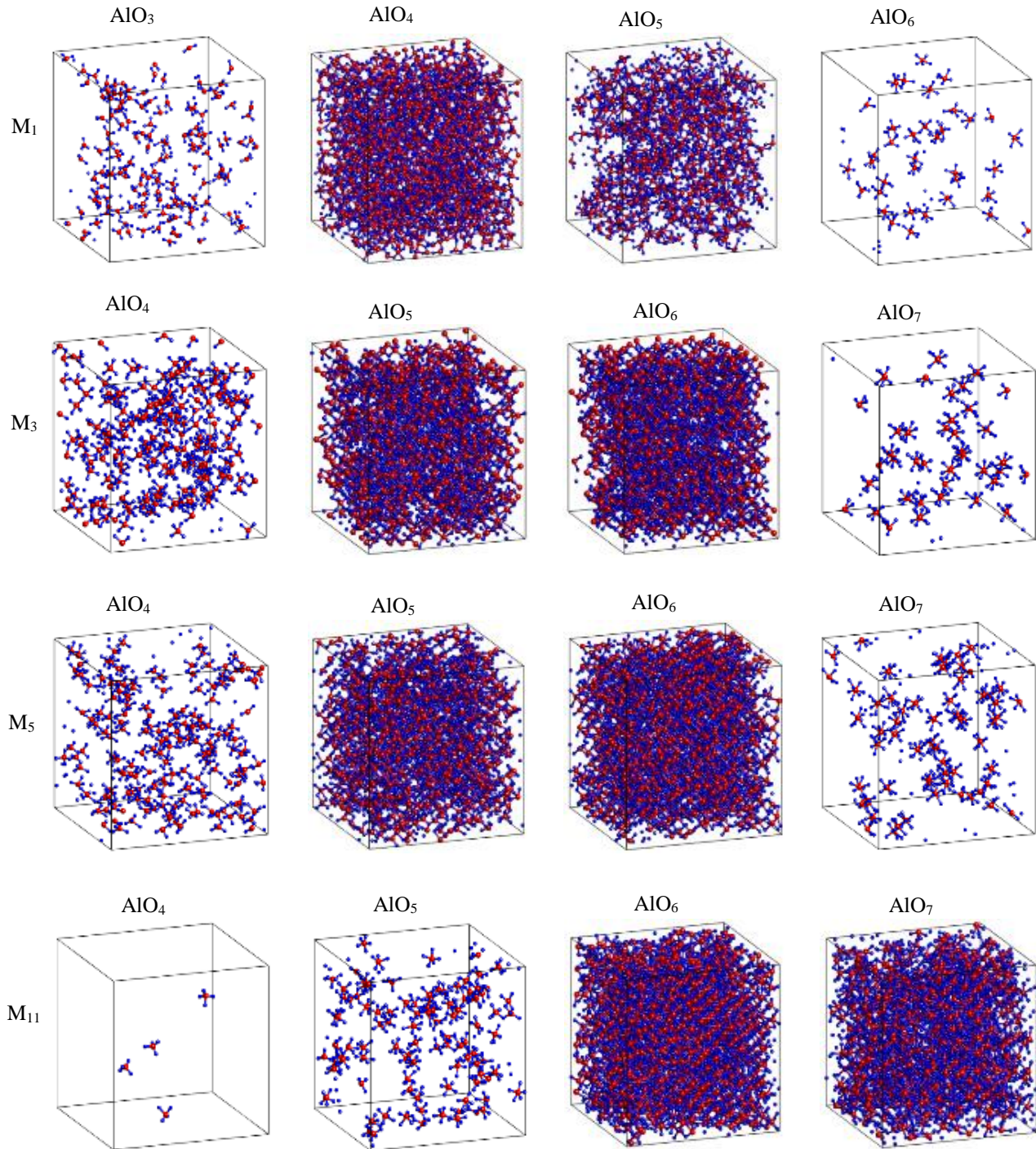
Figure 8. Spatial distribution of AlO$_3$, AlO$_4$, AlO$_5$, AlO$_6$ and AlO$_7$ in the liquid Al$_2$O$_3$ at different pressure and 3500 K. Al and O atoms are in red and blue color, respectively

Further, the network topology, the immediate structural phase and SH can be analyzed by the corner-sharing, the edge-sharing, the face-sharing bonds and their clustering behavior. The distribution of corner-, edge- and face-sharing links (CSL, ESL and FSL) are calculated using the following algorithm: If Al atom connects with Al atom via one bridge O atom, which can be regarded as a corner-sharing bond (Al-O-Al). Also, Al atom connects to Al atom through two bridge O atoms, which is defined as an edge-sharing bond (Al-O-,-O-Al). In case of Al atom connects with Al atom via three bridge O atoms, which is defined as a face-sharing bond (Al-O-,-O-,-O-Al). The employed calculated algorithm is similar with that in Guignard & Cormier (2008) study [31].
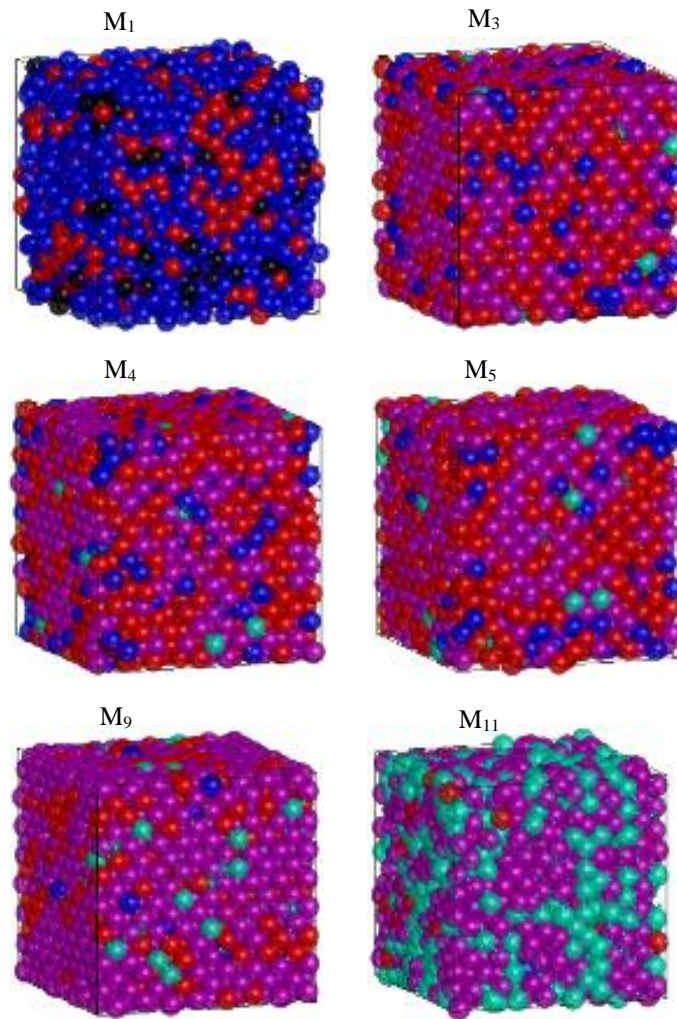
Figure 9. Snapshots of spatial distribution of AlO$_3$ units (in black spheres), AlO$_4$ (in blue spheres), AlO$_5$ (in red spheres), AlO$_6$ (in pink spheres) and AlO$_7$ (in turquoise spheres) for liquid Al$_2$O$_3$ at pressures of 0, 10, 15, 20, 60 and 100 GPa (M$_1$, M$_3$, M$_4$, M$_5$, M$_9$, M$_{11}$) and 3500 K.

Figure 10 displays the spatial distribution of CSL, ESL and FSL of liquid Al$_2$O$_3$. It can be observed that the distribution of CSL, ESL and FSL is not uniform. Obviously, this phenomenon represents structural heterogeneity in liquid Al$_2$O$_3$. In principle, the clusters of face-sharing links form immobile regions and the clusters of corner-sharing links, corresponding mobile regions. The mentioned analysis demonstrated that the coexistence of separate structural phases in network forming is origin of spatially SH with micro-scaled phase separation in liquid Al$_2$O$_3$.
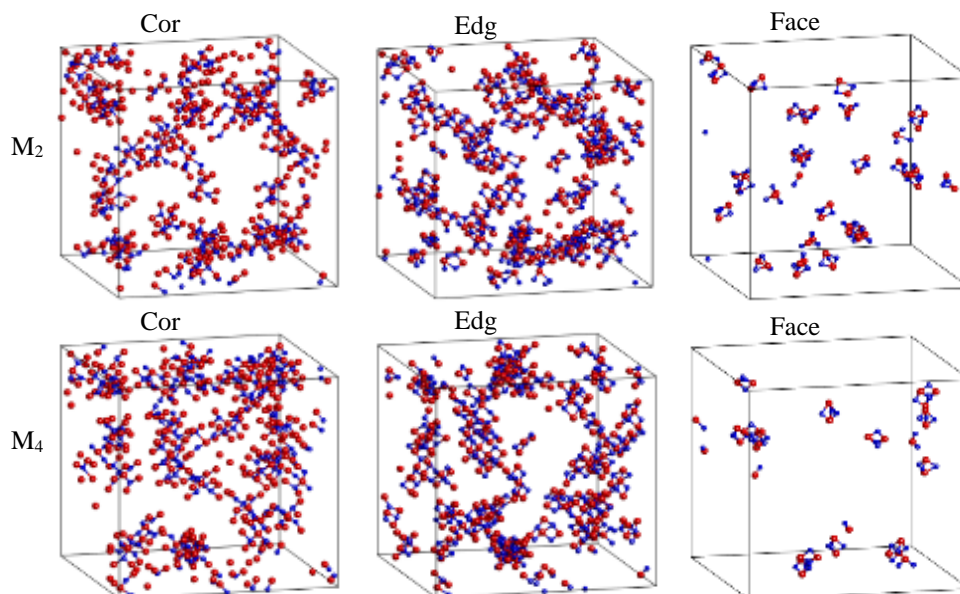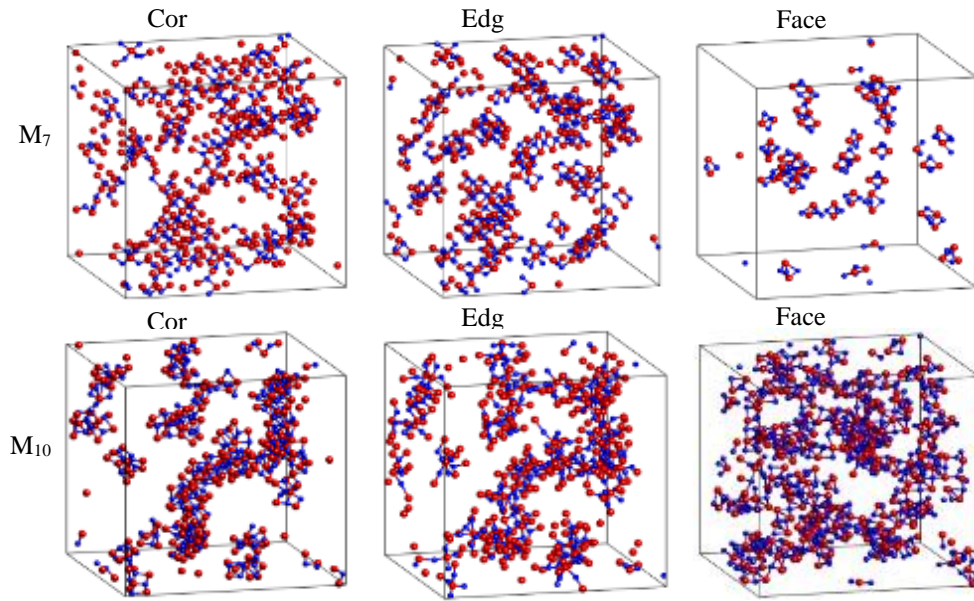
Figure 10. Distribution of corner, edge, face-sharing of Al₂O₃ at pressure of 5, 15, 30 and 80 GPa and 3500 K. Al and O atoms are in red and blue color, respectively

In general, the SH is the main cause of dynamic heterogeneity. Figure 11 shows the mean square displacement (MSD) of Al and O ions as a function of time (at 5, 15, 20, 80, and 100 GPa). It can be seen that O is always more mobile than Al atoms. Consequently, the O-rich regions will be more mobile than the Al-rich regions. It means that the OAl_1-, OAl_2-cluster is more stable than OAl_3-, OAl_4-cluster. This phenomenon confirmed the dynamics of OAl_y-clusters is very interested.
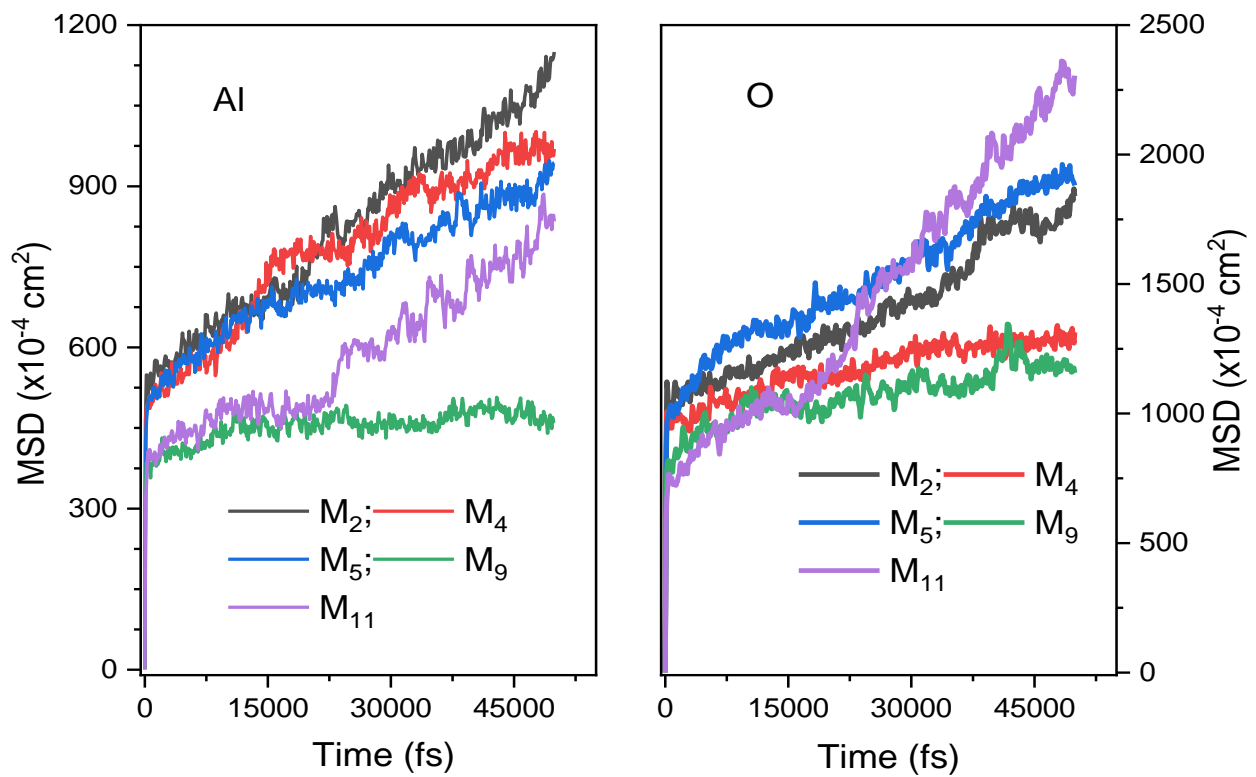

Figure 11. MSD of Al (left) and O (right) atom as a function of time at pressure of 5, 15, 20, 60 and 100 GPa

4. Conclusion

The structural transition and SH under compression are investigated in detail. The obtained result realized the structure organization of liquid Al_2O_3 comprises AlO_3, AlO_4-, AlO_5-, AlO_6 or AlO_7- phases, which depend on the applied pressure. At lower pressures, liquid Al_2O_3 comprises two main AlO_4-, AlO_5-phases and scattering AlO_3-, AlO_6-, AlO_7-phases. In the range of 10-20 GPa, two main AlO_5-, AlO_6- and scattering AlO_3-, AlO_4-, AlO_7-phases are comprised. In case of beyond 20 GPa, two main AlO_6-, AlO_7- and scattering AlO_3-, AlO_4-, AlO_5-phases are comprised. Under compression conditions, the topology of AlO_x is slightly changed and distorted. In the AlO_3- and AlO_4-phases, the AlO_3- and AlO_4-units mainly link to each other through the corner-sharing bonds, for AlO_5-, AlO_6-, AlO_7-phases through corner-, edge-, face-sharing bonds. The existence of separate phases is evidence of SH in liquid Al_2O_3. Furthermore, the Voronoi volumes of O atoms are detected to decrease faster than those of Si, indicating the existence of free-volume regions in liquid Al_2O_3. The atoms in AlO_3-, AlO_4-phases are more mobile than the ones in AlO_6-, AlO_7-phases. Importantly, at pressure below 10 and beyond 20 GPa, AlO_x units are uniformly distributed. Meanwhile, in the range of 10-20 GPa, the spatial distribution of AlO_x units is more homogeneous in space.

5. Declarations

5.1. Author Contributions

Conceptualization and methodology, T.T.Q.N.; formal analysis and investigation, P.H.K.; writing—original draft preparation, G.T.T.T.; writing—review and editing, P.H.K. All authors have read and agreed to the published version of the manuscript.

5.2. Data Availability Statement

The data presented in this study are available in article.

5.3. Funding

5.4. Institutional Review Board Statement

Not Applicable

5.5. Declaration of Competing Interest

The authors declare that they have no known competing financial interests or personal relationships that could have appeared to influence the work reported in this paper.

6. References

[1] Landron, C., Hennet, L., Jenkins, T. E., Greaves, G. N., Coutures, J. P., & Soper, A. K. (2001). Liquid alumina: Detailed atomic coordination determined from neutron diffraction data using empirical potential structure refinement. Physical Review Letters, 86(21), 4839–4842. doi:10.1103/PhysRevLett.86.4839.

[2] Neuville, D. R., Ligny, D. de, Cormier, L., Henderson, G. S., Roux, J., Flank, A.-M., & Lagarde, P. (2009). The crystal and melt structure of spinel and alumina at high temperature: An in-situ XANES study at the Al and Mg K-edge. Geochimica et Cosmochimica Acta, 73(11), 3410–3422. doi:10.1016/j.gca.2009.02.033.

[3] Krishnan, S., Ansell, S., & Price, D. L. (1998). X-ray diffraction from levitated liquid yttrium oxide. Journal of the American Ceramic Society, 81(7), 1967–1969. doi:10.1111/j.1151-2916.1998.tb02578.x.

[4] Kovarik, L., Bowden, M., & Szanyi, J. (2021). High temperature transition aluminas in δ-Al2O3/θ-Al2O3 stability range: Review. Journal of Catalysis, 393, 357–368. doi:10.1016/j.jcat.2020.10.009.

[5] Shi, C., Alderman, O. L. G., Berman, D., Du, J., Neuefeind, J., Tamalonis, A., Weber, J. K. R., You, J., & Benmore, C. J. (2019). The structure of amorphous and deeply supercooled liquid alumina. Frontiers in Materials, 6, 38. doi:10.3389/fmats.2019.00038.

[6] Jahn, S., & Madden, P. A. (2007). Structure and dynamics in liquid alumina: Simulations with an ab initio interaction potential. Journal of Non-Crystalline Solids, 353(32-40), 3500–3504. doi:10.1016/j.jnoncrysol.2007.05.104.

[7] Gutiérrez, G., Belonoshko, A. B., Ahuja, R., & Johansson, B. (2000). Structural properties of liquid [Formula Presented] A molecular dynamics study. Physical Review E - Statistical Physics, Plasmas, Fluids, and Related Interdisciplinary Topics, 61(3), 2723–2729. doi:10.1103/PhysRevE.61.2723.

[8] Verma, A. K., Modak, P., & Karki, B. B. (2011). First-principles simulations of thermodynamical and structural properties of liquid Al2O3 under pressure. Physical Review B - Condensed Matter and Materials Physics, 84(17), 174116. doi:10.1103/PhysRevB.84.174116.

[9] He, D., Liu, F., Guan, S., & He, D. (2021). High-pressure work hardening of alumina. Ceramics International, 47(14), 19989–19994. doi:10.1016/j.ceramint.2021.04.009.

[10] Waseda, Y., Sugiyama, K., & Toguri, J. M. (1995). Direct Determination of the Local Structure in Molten Alumina by High Temperature X-Ray Diffraction. Zeitschrift Fur Naturforschung - Section A Journal of Physical Sciences, 50(8), 770–774. doi:10.1515/zna-1995-0809.

[11] Ansell, S., Krishnan, S., Weber, J. K. R., Felten, J. J., Nordine, P. C., Beno, M. A., Price, D. L., & Saboungi, M. L. (1997). Structure of liquid aluminum oxide. Physical Review Letters, 78(3), 464–466. doi:10.1103/PhysRevLett.78.464.

[12] Hennet, L., Thiaudière, D., Gailhanou, M., Landron, C., Coutures, J. P., & Price, D. L. (2002). Fast x-ray scattering measurements on molten alumina using a 120° curved position sensitive detector. Review of Scientific Instruments, 73(1), 124. doi:10.1063/1.1426228.

[13] Hemmati, M., Wilson, M., & Madden, P. A. (1999). Structure of liquid Al2O3 from a computer simulation model. Journal of Physical Chemistry B, 103(20), 4023–4028. doi:10.1021/jp983529f.

[14] Ahuja, R., Belonoshko, A. B., & Johansson, B. (1998). Melting and liquid structure of aluminum oxide using a molecular-dynamics simulation. Physical Review E - Statistical Physics, Plasmas, Fluids, and Related Interdisciplinary Topics, 57(2), 1673–1676. doi:10.1103/PhysRevE.57.1673.

[15] Hoang, V. Van, & Oh, S. K. (2004). Molecular dynamics study of aging effects in supercooled [Formula Presented]. Physical Review E - Statistical Physics, Plasmas, Fluids, and Related Interdisciplinary Topics, 70(6), 8. doi:10.1103/PhysRevE.70.061203.

[16] Kien, P. H., An, P. M., Trang, G. T. T., & Hung, P. K. (2019). The structural transition under compression and correlation between structural and dynamical heterogeneity for liquid Al2O3. International Journal of Modern Physics B, 33(31), 1950380. doi:10.1142/S0217979219503806.

[17] Vashishta, P., Kalia, R. K., Nakano, A., & Rino, J. P. (2008). Interaction potentials for alumina and molecular dynamics simulations of amorphous and liquid alumina. Journal of Applied Physics, 103(8), 83504. doi:10.1063/1.2901171.

[18] Hong, N. V., Vinh, L. T., Hung, P. K., Dung, M. V., & Yen, N. V. (2019). The structural transition under densification and the relationship between structure and density of silica glass. European Physical Journal B, 92(8), 1–7. doi:10.1140/epjb/e2019-100137-7.

[19] Hoang, V. Van, & Oh, S. K. (2005). Computer simulation of the structural transformation in liquid Al2O3. Journal of Physics Condensed Matter, 17(19), 3025–3033. doi:10.1088/0953-8984/17/19/016.

[20] Skinner, L. B., Barnes, A. C., Salmon, P. S., Hennet, L., Fischer, H. E., Benmore, C. J., Kohara, S., Weber, J. K. R., Bytchkov, A., Wilding, M. C., Parise, J. B., Farmer, T. O., Pozdnyakova, I., Tumber, S. K., & Ohara, K. (2013). Joint diffraction and modeling approach to the structure of liquid alumina. Physical Review B - Condensed Matter and Materials Physics, 87(2), 24201. doi:10.1103/PhysRevB.87.024201.

[21] San Miguel, M. A., Fernández Sanz, J., & Álvarez, L. J. (1998). Molecular-dynamics simulations of liquid aluminum oxide. Physical Review B - Condensed Matter and Materials Physics, 58(5), 2369–2371. doi:10.1103/PhysRevB.58.2369.

[22] Van Hoang, V. (2005). About an order of liquid-liquid phase transition in simulated liquid Al2O3. Physics Letters, Section A: General, Atomic and Solid State Physics, 335(5–6), 439–443. doi:10.1016/j.physleta.2004.12.040.

[23] Hung, P. K., & Vinh, L. T. (2008). Local microstructure of amorphous Al2O3. Physica Status Solidi (B) Basic Research, 245(5), 950–958. doi:10.1002/pssb.200844047.

[24] Hong, N. V., Lan, M. T., Nhan, N. T., & Hung, P. K. (2013). Polyamorphism and origin of spatially heterogeneous dynamics in network-forming liquids under compression: Insight from visualization of molecular dynamics data. Applied Physics Letters, 102(19), 191908. doi:10.1063/1.4807134.

[25] Ha, N. T. T., Hong, N. V., & Hung, P. K. (2019). Network structure and dynamics heterogeneities in Al2O3 system: insight from visualization and analysis of molecular dynamics data. Indian Journal of Physics, 93(8), 971–978. doi:10.1007/s12648-018-01358-7.

[26] Belashchenko, D. K. (1997). Computer simulation of the structure and properties of non-crystalline oxides. Russian Chemical Reviews, 66(9), 733–762. doi:10.1070/rc1997v066n09abeh000236.

[27] Hung, P. K., Vinh, L. T., Hong, N. V., Thu Ha, N. T., & Iitaka, T. (2018). Two-domain structure and dynamics heterogeneity in a liquid SiO2. Journal of Non-Crystalline Solids, 484, 124–131. doi:10.1016/j.jnoncrysol.2018.01.023.

[28] Lan, M. T., Thi Thanh Ha, N., Van Hong, N., & Hung, P. K. (2019). Structure and dynamical heterogeneity in GeO2 liquid: a new approach. European Physical Journal B, 92(6), 1–7. doi:10.1140/epjb/e2019-100021-6.

[29] Salmon, P. S., Drewitt, J. W. E., Whittaker, D. A. J., Zeidler, A., Wezka, K., Bull, C. L., Tucker, M. G., Wilding, M. C., Guthrie, M., & Marrocchelli, D. (2012). Density-driven structural transformations in network forming glasses: A high-pressure neutron diffraction study of GeO 2 glass up to 17.5GPa. Journal of Physics Condensed Matter, 24(41), 415102. doi:10.1088/0953-8984/24/41/415102.

[30] Biswas, P., Atta-Fynn, R., & Drabold, D. A. (2004). Reverse Monte Carlo modeling of amorphous silicon. Physical Review B - Condensed Matter and Materials Physics, 69(19), 195207. doi:10.1103/PhysRevB.69.195207.

[31] Guignard, M., & Cormier, L. (2008). Environments of Mg and Al in MgO-Al2O3-SiO2 glasses: A study coupling neutron and X-ray diffraction and Reverse Monte Carlo modeling. Chemical Geology, 256(3–4), 111–118. doi:10.1016/j.chemgeo.2008.06.008.